Journal of Cleaner Production 247 (2020) 119177

Contents lists available at ScienceDirect

Journal of Cleaner Production

journal homepage: www.elsevier.com/locate/jclepro

Utilization of urea as an accessible superplasticizer on the moon for lunar geopolymer mixtures

Shima Pilehvar [a], Marlies Arnhof [b], Ramón Pamies [c], Luca Valentini [d], Anna-Lena Kjøniksen [a, *]

[a] Faculty of Engineering, Østfold University College, P.O. Box 700, 1757, Halden, Norway
[b] Advanced Concepts Team, ESA European Space Research and Technology Centre, Keplerlaan 1, TEC-SF, 2201AZ, Noordwijk, Netherlands
[c] Department of Materials Engineering and Manufacturing, Technical University of Cartagena, Cartagena, Murcia, Spain
[d] Department of Geosciences, University of Padua, 35131, Padua, Italy

ARTICLE INFO

Article history:
Received 2 July 2019
Received in revised form
24 September 2019
Accepted 4 November 2019
Available online 5 November 2019

Handling editor: Panos Seferlis

Keywords:
Geopolymer
Lunar regolith simulant
Urea
Superplasticizer
Lunar construction

ABSTRACT

When developing materials for lunar construction, it is essential to minimize the weight of components that have to be brought in from Earth. All necessary ingredients for geopolymers could potentially be sourced on the lunar surface, which is why the material might be an efficient construction material for infrastructure on the moon. Finding a chemical admixture that can be easily obtained on the moon, which can increase the workability while utilizing less water, would be highly beneficial for utilizing lunar regolith geopolymers for lunar 3D printing. Urea can break hydrogen bonds, and therefore reduces the viscosities of many aqueous mixtures. Since urea is the second most abundant component in urine (after water), it is readily available anywhere there are humans. We have therefore explored the possibility of utilizing urea as a chemical admixture for lunar geopolymers. Addition of urea has been compared with polycarboxylate and naphthalene based superplasticizers, and with a control mixture without superplasticizer. When curing the sample containing urea at 80 °C, the initial setting time became longer. The samples containing urea or naphthalene-based superplasticizers could bear heavy weights shortly after mixing, while keeping an almost stable shape. Samples without superplasticizer or containing the polycarboxylate-based admixture were too stiff for mold-shaped formation after casting. Samples containing urea and naphthalene-based admixtures could be used to build up a structure without any noticeable deformation. Initial compressive strength of the samples with urea was higher than for the two other specimens containing superplasticizers, and it continued to rise even after 8 freeze-thaw cycles. Microstructural studies revealed that superplasticizers can influence the formation of additional air voids within the samples.

1. Introduction

With a growing interest in the human exploration of celestial bodies, establishing *in-situ* habitats on the lunar surface may facilitate surveys further away from the Earth by providing an important extra-terrestrial base (Happel, 1993). However, colonizing the moon poses several problems such as high radiation levels, extreme temperatures and large temperature fluctuations, vacuum, and meteoroids (Benvenuti et al., 2013). According to the National Aeronautics and Space Administration (NASA), transporting one pound (0.45 kg) of materials into orbit costs around $10,000 USD (Qiu and Park, 2001). Therefore, to keep the transportation costs feasible, both NASA and the European Space Agency (ESA) promote the use of *in-situ* materials (Leach, 2014).

Utilizing lunar surface materials to fabricate cement/concrete for *in-situ* construction has been proposed previously (Buchner et al., 2018; Cesaretti et al., 2014). Cesaretti et al. (2014) proposed a D-shape 3D printing process with Sorel cement for construction on the lunar surface. Unfortunately, the process required substantial amounts of consumables (chemicals and water) to produce the binder. Buchner et al. (2018) developed a rock-like material by using phosphoric acid as a liquid binder. For lunar applications, considerable amounts of water and phosphoric acid would have to be transported to the lunar surface. However, this material seems to

* Corresponding author.
E-mail address: anna.l.kjoniksen@hiof.no (A.-L. Kjøniksen).

https://doi.org/10.1016/j.jclepro.2019.119177

be promising for use on the Martian surface, as phosphoric acid and water are available on Mars. Since water is a highly valuable resource on the lunar surface and not readily available (Hauri et al., 2015), using building materials with high water demand is practically impossible. Geopolymers consist of silico-aluminates in an amorphous to semi-crystalline three-dimensional structure. Geopolymers exhibit an excellent performance such as quick controllable setting and hardening (Hardjito et al., 2008; Li et al., 2004), high compressive strength (Allahverdi et al., 2016; Ryu et al., 2013), freeze-thaw resistance (Fu et al., 2011; Sun and Wu, 2013), excellent durability in sulfate environment and superior resistance to acid and salt attacks (Bakharev, 2005a, b), high fire resistance and low thermal conductivity (Cheng and Chiu, 2003; Kong and Sanjayan, 2010), small shrinkage (Ana M. Fernandez-Jimenez and Cecilio, 2006) and adequate radiation shielding (Montes et al., 2015). Geopolymerization of lunar regolith has therefore been proposed due to the high amounts of aluminosilicates at a similar ratio as the main components of traditional geopolymer binders, and the favorable shielding properties for a crew inside the lunar construction (Montes et al., 2015). Additionally, the presence of alkali metals on the moon might be used as a source of the alkaline solution for geopolymerization (Matta et al., 2009). Utilization of lunar regolith and alkali metals as the components of geopolymer composites can thereby facilitate lunar construction without the need of bringing materials in from the Earth at extreme cost.

Recently, 3D printing technology has been developed in large scale to allow direct construction of buildings (Buswell et al., 2018; Ceccanti et al., 2010; Ngo et al., 2018). For lunar construction, 3D printing minimizes the involvement of human labor in the building process, reducing health hazards and inefficiencies during construction (Benvenuti et al., 2013). However, in order to utilize 3D printing to build a layer-by-layer structure, the geopolymer composite should exhibit high workability for extrusion, keep its shape after printing, high early concrete strength, and optimal setting time (Le et al., 2012). Fresh geopolymer composites have poor workability due to the higher viscosity of the alkaline solution. Improved workability can be obtained by adding extra water to the mixture. However, water on the moon is not readily available, therefore adding more water to the geopolymer mixture is not realistic (Chua and Johnson, 1998). Additionally, extra water will reduce the compressive strength of geopolymers (Aliabdo et al., 2016). A better way to achieve a good workability is therefore to utilize a low dosage of a chemical admixture. For fly ash based geopolymers, a polycarboxylate-based superplasticizer is preferred when the calcium ion content is relatively high (Xie and Kayali, 2016), while a naphthalene based superplasticizer is effective for low amounts of calcium (Jang et al., 2014; Xie and Kayali, 2016). However, utilizing these superplasticizers in lunar geopolymers would involve transportation from the Earth at great cost. It is therefore preferable to find a superplasticizer that would be available on the moon. The lunar surface is lacking in suitable materials for use as superplasticizers. However, if we assume human presence during construction, we also have access to human waste materials. Human urine contains about 9.3–23.3 g/L urea (Putnam, 1971). It is well known that urea is capable of breaking hydrogen bonds, thereby reducing the viscosities of many aqueous mixtures (Usha and Ramasami, 2002). It is therefore reasonable to assume that urea might work as a superplasticizer to reduce the water demand of the geopolymers.

The objective of this research is to investigate whether urea obtained from humans on the moon can be utilized as a chemical admixture to reduce the water needed to obtain a good workability of lunar regolith geopolymers for 3D printing. The effectiveness of urea as a superplasticizer will be compared to more traditional naphthalene and polycarboxylate based geopolymer superplasticizers. The aim is to develop a lunar regolith geopolymer mixture that can meet the severe curing conditions on the lunar surface (extreme temperature cycles, little available water, and vacuum) without the extreme cost of importing any of the components from the Earth.

2. Experimental

2.1. Materials

DNA-1 lunar regolith simulant developed for ESA as a chemical and mineralogical analog to the lunar mare regolith, has been produced by Dini Engineering srl for Monolite UK ltd in the premises of Cascine di Buti (Pisa), Italy. The chemical composition of this lunar regolith simulant is given in Table 1. The chemical composition of regolith is similar to class F fly ash (Norcem, Germany), which is used for terrestrial geopolymers. However, the percentage of crystalline phase of regolith simulant is 75% whereas 37% crystalline phase was observed for fly ash. As can be seen from Table 1, most of the components of the lunar regolith simulant is within the range found in lunar regolith samples. Fig. 1 show microscopic images (SEM) of the supplied lunar regolith simulant and fly ash (FA) to evaluate the shape difference of the particles. The particle shape of the lunar regolith simulant is angular, simulating the shape of lunar regolith which has been bombardment by meteorites in the lunar environment (Colwell et al., 2007). FA is generally spherical in shape. The size distributions of the lunar regolith simulant and FA determined by low angle laser light scattering (Malvern Mastersizer 2000) are displayed in Fig. 2. The regolith particles have a higher particle size distribution than FA. However, about 30% of the cumulative volume of lunar regolith simulant particles overlap with the size range of FA.

Sodium hydroxide pellets purchased from VWR, Norway, was used for preparing the alkaline solution. In this study, urea (in powder form) supplied by VWR, Norway, was used as an accessible lunar superplasticizer to reduce the amount of water needed to achieve the desired the workability of lunar geopolymer (LG) mixtures. Additionally, naphthalene and polycarboxylate based chemical admixtures (in powder form) were utilized for comparison, since these have been shown to work for other geopolymers previously (Xie and Kayali, 2016). These chemical admixtures are named FLUBE CR 100 F (a poly-naphthalene sulfonate polymer) and SUPLA PDP 2 SA (a polycarboxylic modified polymer), both provided by Bozzetto Group, Italy.

2.2. Mixing, casting and curing procedures

For all LG mixtures, a sodium hydroxide solution 12 M (480 g/L) was selected as an alkaline solution. The alkaline solution was prepared one day in advance to dissolve the NaOH pellets completely in the water and to release the exothermic reaction heat. Laboratory trials of workability and buildability showed that an alkaline solution to regolith ratio of 0.35 and a chemical admixture dosage corresponding to 3% of the lunar regolith mass were optimal. By considering the water limitation and transporting cost for lunar constructions, this step was repeated several times to gain the minimum amounts of alkaline solution and superplasticizer, while keeping the workability and strength at acceptable levels. Accordingly, while about 64 wt% of the alkaline solution is water, the ratio of water to the total mass of geopolymer solids (lunar regolith simulant, NaOH pellets and chemical admixture) is 0.19. The compositions of the mixtures are shown in Table 2.

For specimen preparation, regolith, alkaline solution and one type of chemical admixture were mixed together for 10 min to reach a homogenous and uniform mixture. After mixing, the

Table 1
Chemical composition of DNA-1 lunar regolith simulant and fly ash class F, compared to the composition of lunar regolith samples (the highest and lowest values of each component from 19 analyzed lunar samples is shown).

Chemical	Lunar regolith simulant DNA-1 (wt. %)	Fly ash class F (wt. %)	Lunar regolith soil samples range (wt. %) (McKay et al., 1991)
SiO_2	47.79 ± 0.05	50.83 ± 0.04	40.6–48.1
Al_2O_3	19.16 ± 0.07	23.15 ± 0.06	12.0–28.0
Fe_2O_3	8.75 ± 0.01	6.82 ± 0.01	4.7–19.8
CaO	8.28 ± 0.03	6.87 ± 0.02	10.3–15.8
K_2O	3.52 ± 0.02	2.14 ± 0.01	0.04–0.55
Na_2O	4.38 ± 0.03	1.29 ± 0.01	0.31–0.70
MgO	1.86 ± 0.01	1.70 ± 0.01	5.6–13.0
TiO_2	1.00 ± 0.01	1.01 ± 0.01	0.47–8.4

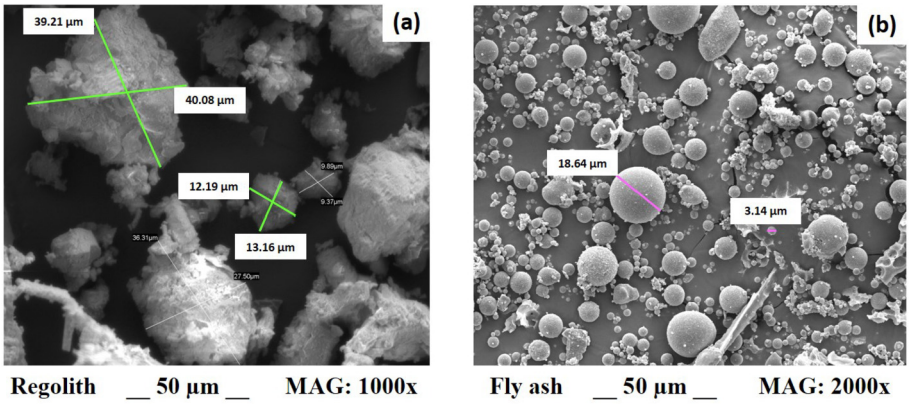

Fig. 1. SEM images of (a) lunar regolith simulant and (b) fly ash.

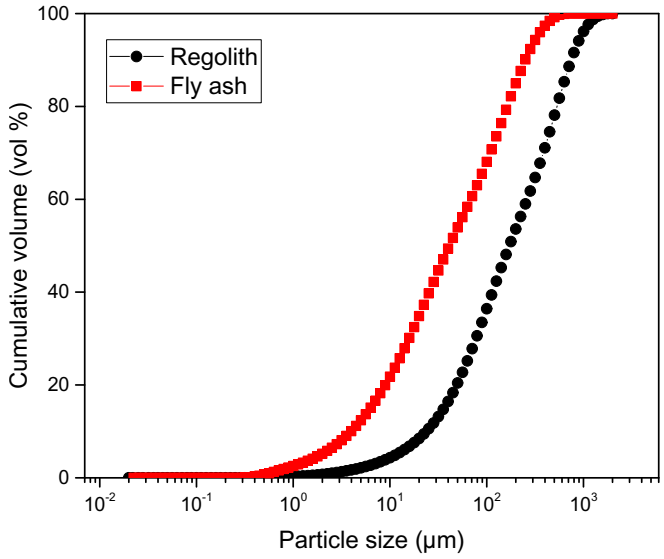

Fig. 2. Particle size distributions of lunar regolith simulant and fly ash.

mixture was cast into molds at a size of $3 \times 3 \times 3\ cm^3$. A vibration machine was used for 1 min to remove air trapped inside the specimens. After casting, LG samples were pre-cured in a heating chamber with a temperature of 80 °C for 6 h. After demolding, the samples were exposed to freeze-thaw cycles. In a single freeze-thaw cycle, the specimens were first placed in the heating chamber at 80 ± 2 °C for 48 h and then the samples were left in a freezer at a temperature of − 80 ± 2 °C for the next 48 h. The samples were subjected to 0, 2, 4 and 8 freeze-thaw cycles.

2.3. Testing methods

2.3.1. Shape deformation and layer-by-layer buildability

The shape deformation was calculated to examine the effect of different chemical admixtures on the shape retention of LG. After molding 200 g mixture with a conical mold, immediately after demolding, 1000 g and 2000 g metal weights were put on top of the fresh samples to evaluate the percentage of sample shape deformation under pressure.

$$Shape\ deformation = \frac{D_{after} - D_{before}}{D_{before}} \times 100$$

where D_{before} and D_{after} are the bottom diameter of the sample before and after demolding, respectively. D_{before} is 7 cm for all samples, which is the inside diameter of conical mold bottom. After the shape deformation evaluation, only mixtures with useable workability and with high shape retention were selected for the layer-by-layer buildability test. The buildability of LG mixtures was

Table 2
Composition of mixture design for LG. The percentage of chemical admixtures is calculated according to the mass of lunar regolith simulant.

Name of mixture	$NaOH_{(aq)}$/Regolith	Chemical admixture
W/O	0.35	–
U	0.35	Urea - 3%
C	0.35	polycarboxylate based (SUPLA PDP 2 SA) - 3%
N	0.35	naphthalene based(FLUBE CR 100 F) - 3%

examined by means of a high-pressure syringe pump (Fusion 6000, Chemyx, Inc.) with a constant pump rate of 20 ml/min (Fig. 3).

2.3.2. Setting time

To characterize the initial and final setting times of LG after adding three different chemical admixtures, a Vicat needle test was performed by a manual Vicat needle apparatus in accordance with EN 196-3. After placing the fresh mixture in the conical metal mold, the mold was transferred to the heating chamber at 80 °C. Setting time measurements were carried out at 80 °C with an interval of 15 min. The initial setting time is the time when the needle penetration is less than 39 mm whereas the final setting time is the moment when the needle penetrates the sample to a depth of 0.5 mm.

2.3.3. Compressive strength

The compressive strength tests for LG specimens after 0, 2, 4, and 8 freeze-thaw cycles were performed at 20 °C in accordance with EN 12190, using a digital compressive strength test machine (Form + Test Machine).

2.3.4. FTIR

LG specimens after 0, 4 and 8 freeze-thaw cycles were characterized via Fourier-Transform Infrared Spectroscopy (FTIR). FTIR analysis was conducted with a spectrometer (PerkinElmer Spectrum BX) in transmittance mode from 4000 to 500 cm^{-1}. Samples were dried before measurement at 80 °C for 12 h.

2.3.5. X-ray tomography

X-ray microtomography (XCT) scans were performed on drill cores of samples after 0 and 4 freeze-thaw cycles. These cylindrical samples have a diameter of 1 cm and a height of approximately 2 cm. The analyses were performed using a Skyscan 1172 XCT scanner, with an energy of 100 kV, 0.9 s acquisition time and 0.3° rotation step. Tomographic reconstruction was performed using the FDK algorithm (Feldkamp et al., 1984). The reconstructed images consist of 1200 vertically stacked cross-sections, with a linear pixel size of 6.5 μm. Image processing, including binary segmentation and particle analysis, was performed by the ImageJ software (Schneider et al., 2012), by which the size of not interconnected pores was measured. In order to estimate the accuracy and error associated with the image processing procedure, a random distribution of spherical pores with known particle size was generated. After addition of gaussian noise, the image was binarized and the total porosity and sphere radius was compared with those relative to the original image. The average errors associated with porosity and pore radius were 4% and 15% respectively.

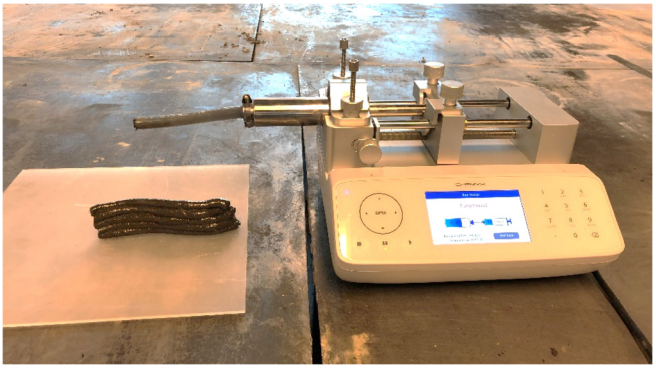

Fig. 3. A high-pressure syringe pump is utilized for 3D-printing the samples.

3. Results and discussion

3.1. Shape deformation and layer-by-layer buildability

One of the most challenging features in 3D concrete printing is that the materials should be able to retain their shape after extruding. Fig. 4 depicts shape deformation of fresh mixtures after placing a 1 kg weight on top of the samples. As can be seen from Fig. 4a and c, fresh W/O and C samples retain a stable shape after loading with a 1 kg weight. However, there are many fractures in the samples, due to the stiffness of the mixtures during mixing and molding. To have a low shape deformation, a mixture should have a good workability and high viscosity. However, the W/O and C samples are too stiff for casting, causing the formation of heterogeneous and fractured structures. It has previously been shown that a polycarboxylate-based superplasticizer (such as the one used in sample C) is often the best choice for fly ash class C, due to the strong bonds between the positively charged calcium and the negatively charged polycarboxylate (Xie and Kayali, 2016). Since the lunar regolith simulant is similar to fly ash class F, this superplasticizer is not optimal for improving the workability and flowability of the mixture. From Fig. 4b and d it is evident that fresh U and N mixtures are castable after molding with a smooth surfaces with none (U sample) or few (N sample) fractures. These samples also retain their shape under a 1 kg external load. Accordingly, mixture U and N were selected for further studies.

In the next step, a 2 kg weight was placed on top of the fresh U and N mixtures for shape deformation evaluation (Fig. 5). The percentage of shape deformation was 11.4% and 13% for the U and N mixtures, respectively. Accordingly, the sample containing urea

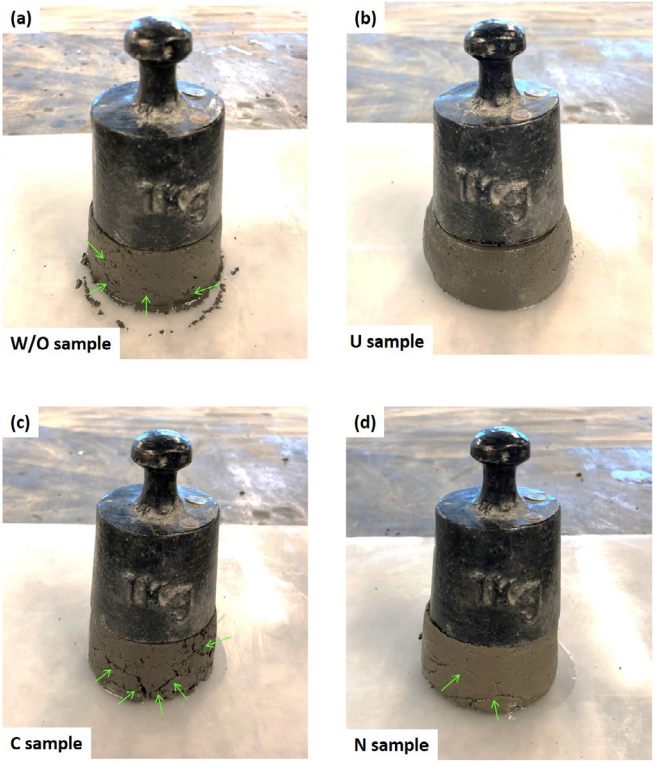

Fig. 4. Sample retention after loading a 1 kg weight over (a) mixture without any admixture (W/O sample), (b) mixture containing 3% urea (U sample), (c) mixture containing 3% polycarboxylate-based admixture (C sample), and (d) and mixture containing 3% naphthalene-based admixture (N sample). The arrows show fractures and disruptions formed during molding.

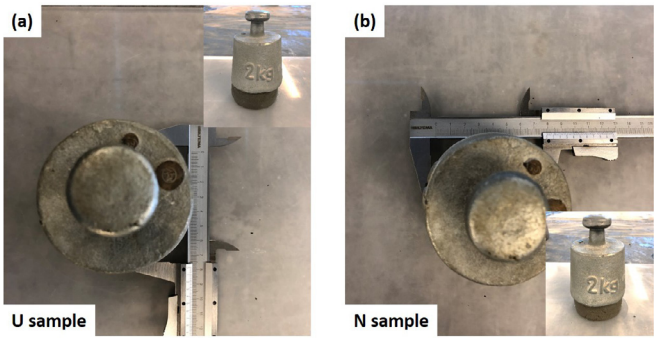

Fig. 5. Sample deformation after loading a 2 kg weight over (a) mixture containing 3% urea (U sample), (b) mixture containing 3% naphthalene-based admixture (N sample).

retains its shape better after loading with a weight that is 10 times that of the 200 g sample.

In Fig. 6, layer-by-layer buildability was measured by means of a syringe pump for selected mixtures (U and N) to see how many layers is possible to stack without any deformation of the layers or collapse of the structure, and without utilizing a rest time between layers. Due to the narrow extruding tube (1 cm in diameter), only 4 and 5 layers of filament were built up for the U and F samples, respectively. As can be seen from Fig. 6, there are slight changes of the thickness of each layer. However, all the layers are nicely vertically stacked, and remain steady without any obvious deformation and collapse. Accordingly, urea and the naphthalene-based admixture can contribute positively to the buildability of the LG.

3.2. Setting time

Fig. 7 shows the effect of different superplasticizers on the initial and final setting times of lunar geopolymer at 80 °C. The three superplasticizers influence the setting times in different ways. Incorporating 3% urea (U) postpones both initial and final setting times in comparison with the sample without any chemical admixture (W/O). For both mixtures containing 3% polycarboxylate-based admixture (C) and naphthalene-based admixture (N), there is a moderate delay of the initial setting time, while a much longer final setting time was observed for the N mixture. In 3D printing, the time after mixing until the fresh material losses the workability for extruding is called the open time. The open time is always earlier than the initial setting time (Panda and Tan, 2018). Therefore, a longer initial setting time will help maintain a continuous flow during pumping, and prevent the material from becoming too hard in the 3D printer. For good shape retention during layer-by-layer buildability, the fresh LG mixture should gain high early strength after extrusion to tolerate subsequent layers resting on top (Ngo et al., 2018). Acceptable final setting time is therefore an advantage to allow the LG layers to be loaded onto the previous layers without shape deformation. Accordingly, the mixture containing urea exhibits the best initial and final setting times for 3D printing.

3.3. Compressive strength

The compressive strength of the samples after 0, 2, 4 and 8 freeze-thaw cycles is shown in Fig. 8. The sample without any chemical admixture exhibits the highest compressive strength after 8 freeze-thaw cycles (32 MPa). As mentioned previosly, for 3D printing high early strength is needed after extrusion to tolerate the weight of subsequent layers loaded on top of the sample. The C and N samples show a low early strength of about 1.7 MPa, which is not optimal for 3D printing. Interestingly, the U sample exhibited a relatively high initial compressive strength (13 MPa) after precuring at 80 °C.

During the freeze-thaw cycles, two opposing mechanisms are affecting the compressive strength. The freeze thaw cycles are expected to reduce the compressive strength due to expansion of water within the samples when it freezes, which may cause fractures within the samples. At the same time, the geopolymerization reaction within the samples continues, which will increase the compressive strength. This results in a continous slight increase in compressive strength for the U sample. For the three other samples the competing mechanisms causes a variation in compressive strength over the freeze thaw cycles, but with an overall strong increase from 0 to 8 cycles. The compressive strength requirement for lunar construction is 1/6 of the requirement of a similar structure on Earth (Montes et al., 2015), which is normally around 25–40 MPa (Kosmatka et al., 2002). Except for the C and N samples before the freeze-thaw cycles, all samples are well above this limit (>7 MPa).

After 8 freeze-thaw cycles, the U and N samples have approximately the same compressive strength, while the sample without superplasticizer has a much higher compressive strength. The C-sample has a large variation between the three tested cubes, but seems to have a strength somewhere between the other samples. Interestingly, the samples with the lowest compressive strength after 8 freeze-thaw cycles (U and N) are the same ones that are best suited for 3D-printing (Figs. 4 and 6). In order to explore the mechanisms behind the differences, FT'IR and X-ray microtomography experiments have been performed.

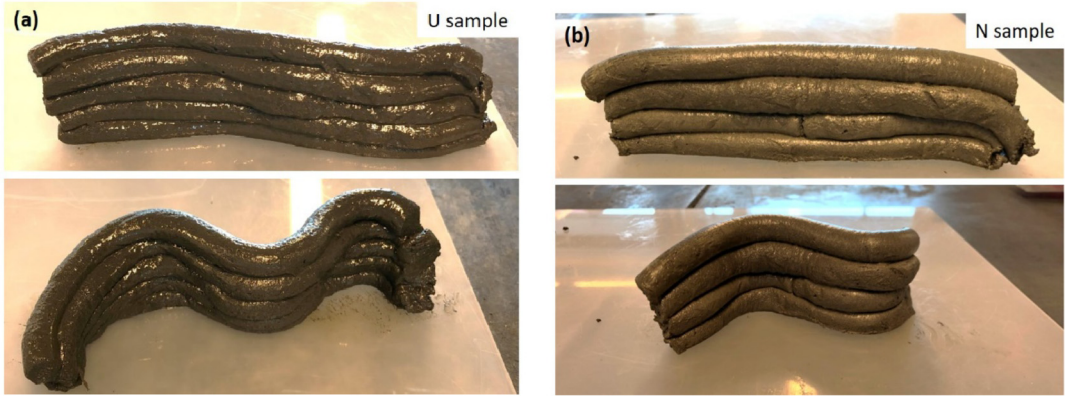

Fig. 6. Layer-by-layer buildability of (a) mixture containing 3% urea (U sample), (b) mixture containing 3% naphthalene-based admixture (N sample).

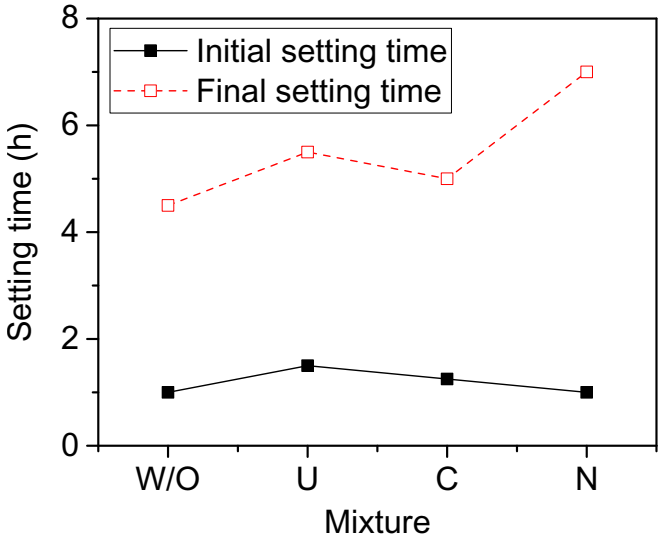

Fig. 7. The initial and final setting times of W/O (without any admixture), U (urea), C (polycarboxylate-based admixture) and N (naphthalene-based admixture) lunar geopolymer mixtures.

3.4. FTIR

Fig. 9 presents the FTIR spectra of the four different LGs after 0, 4, and 8 freeze-thaw cycles. The main band is centered around 975 cm^{-1} and corresponds to asymmetric stretching vibration of Si–O–T (T = Si or Al) (Abdullah et al., 2012; Rees et al., 2007a; 2007b). This peak indicates the degree of amorphous aluminosilicate gel phase due to dissolution of the regolith in the alkaline solution (Abdullah et al., 2012). After 0 freeze-thaw cycles, this peak is strongest for the W/O and U samples, which is in agreement with the higher compressive strengths of these samples at this stage (Fig. 8). After 4 freeze-thaw cycles (Fig. 10b), the C sample exhibited the highest amount of geopolymer gel formation resulting in a broader and deeper peak. In contrast, the sample containing urea (U) exhibited the smallest amount of gel which resulted the lowest compressive strength after 4 freeze-thaw cycles (Fig. 8). Interestingly, after 8 freeze-thaw cycles, the U sample revealed similar intensity and depth of this peak as the C sample, which indicate a

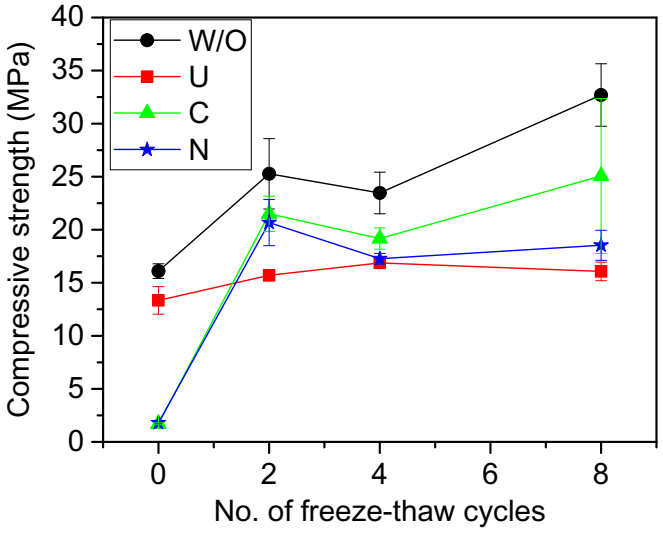

Fig. 8. Compressive strength of lunar geopolymer versus the number of freeze-thaw cycles containing 0 wt% of superplasticizer (W/O) and 3 wt% of urea (U), 3% polycarboxylate-based admixture (C), and 3% naphthalene-based admixture (N). The samples were pre-cured for 6 h at 80 °C before starting the freeze thaw cycles.

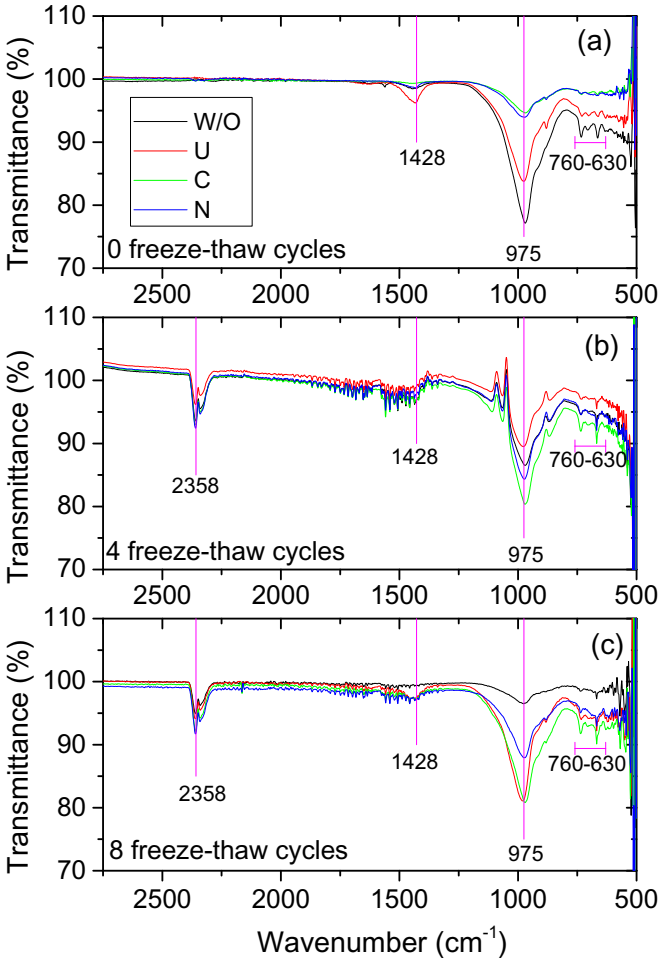

Fig. 9. FTIR spectra of lunar Geopolymer specimens containing 0 wt% superplasticizer (W/O) and 3 wt% of urea (U), 3% polycarboxylate-based admixture (C), and 3% naphthalene-based admixture (F)(a) after 0 freeze-thaw cycles and (b) after 4 freeze-thaw cycles, and (c) after 8 freeze-thaw cycles.

continuing formation of geopolymeric products after 8 freeze-thaw cycles.

The broad IR band at around 2358 cm^{-1} (after 4 and 8 freeze-thaw cycles) is related to the bending vibration of H–O–H bonds from weakly bound water molecules (Abdullah et al., 2012). Since this peak is not evident before the freeze-thaw cycles, this is probably from water adsorbed onto the samples during the freeze-thaw process.

The small peaks at 1428 cm^{-1} has been attributed to stretching vibrations of O–C–O bonds, which suggests that sodium bicarbonate has been formed due to atmospheric carbonation of the high alkaline NaOH solution (Abdullah et al., 2012). There is a number of smaller peaks in the 630-760 cm^{-1} region, which are contributed to aluminosilicate ring and cage structures (Rees et al., 2007a, 2007b).

3.5. X-Ray tomography

Typical 2D X-ray micro-tomography cross-sectional slices obtained from the W/O, U, C, and N samples after 0 and 4 freeze-thaw cycles are shown in Fig. 10, where cracks and air voids are displayed in dark color (low or no X-ray attenuation). More microcracks are evident in the U matrix after exposure to freeze-thaw cycles. This indicates that the microcracks generated by the freeze-thaw cycles can contribute to the deterioration of the U sample. This is probably

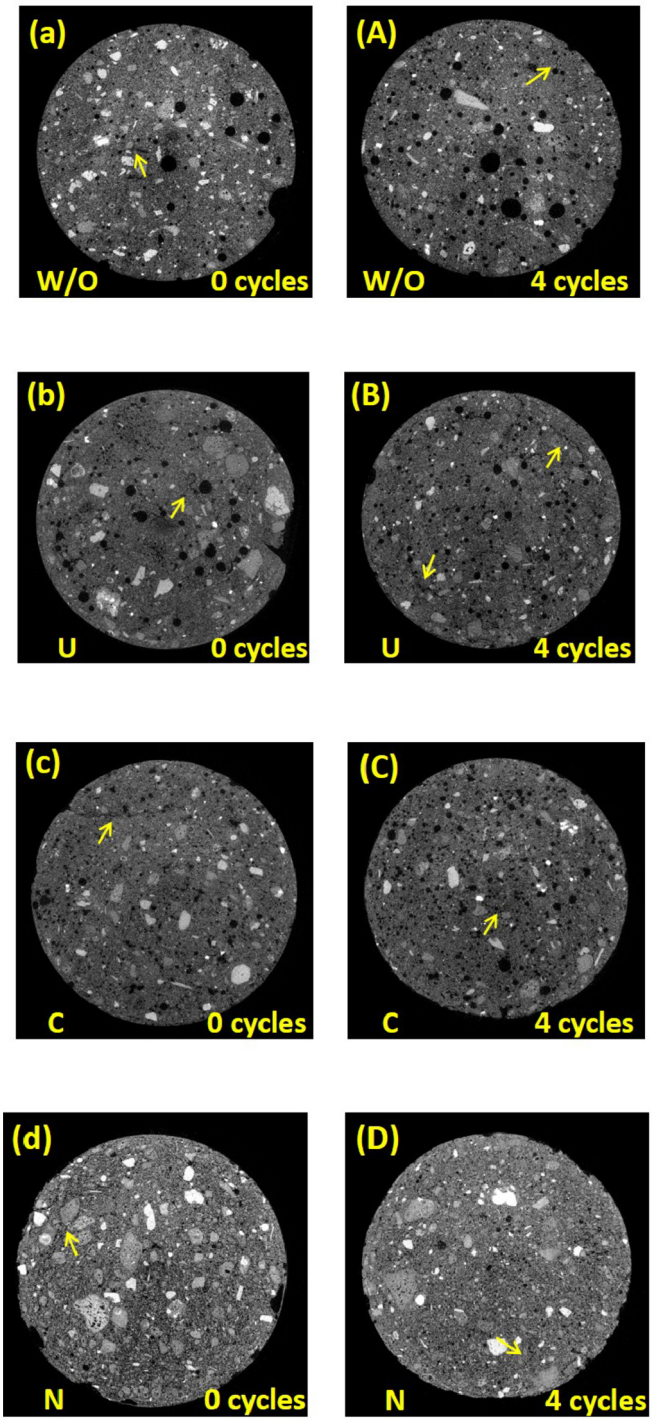

Fig. 10. 2D X-ray tomography images of (a) W/O sample – 0 cycles, (A) W/O sample – 4 cycles, (b) U sample – 0 cycles, (B) U sample – 4 cycles, (c) C sample – 0 cycles, (C) C sample – 4 cycles, (d) N sample – 0 cycles, and (D) N sample – 4 cycles. The arrows show the microcracks in the sample matrix. The field of view is approximately 1 cm.

a contributing factor to the lower compressive strength of this sample after the freeze thaw cycles (Fig. 8).

Fig. 11 illustrates the air voids (in red color) in the 3D images of the samples. In order to quantify the differences, the pore diameter distributions are plotted in Fig. 12 and the volume %, mean diameter, and number of air voids per mm^3 is shown in Fig. 13. Figs. 11 and 13a illustrates that before the freeze-thaw cycles the inclusion of urea (U) and the polycarboxylate-based admixture (C) led to a substantial increase of porosity in comparison with the sample

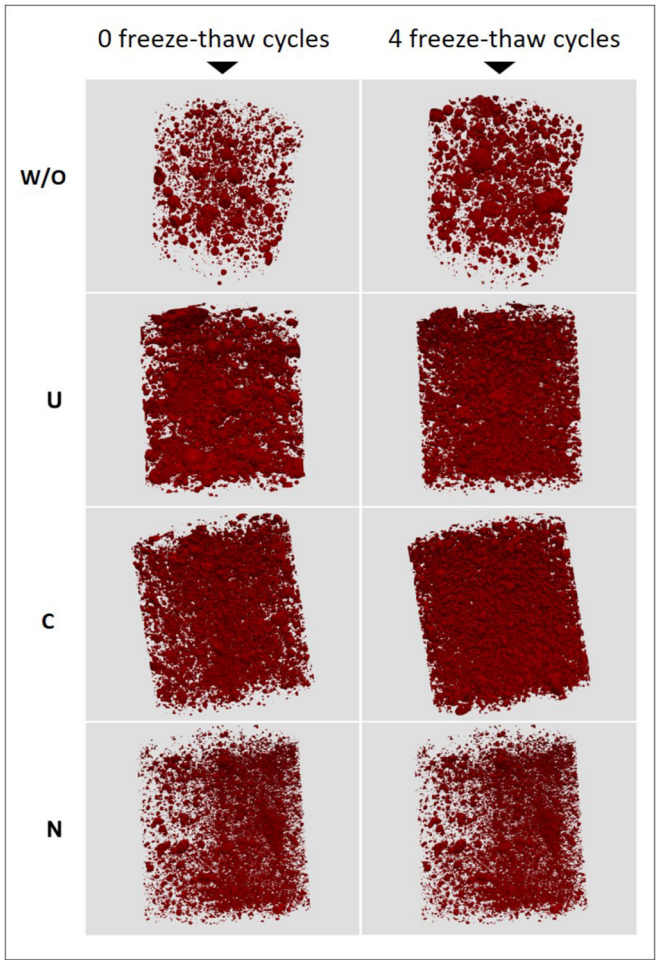

Fig. 11. 3D X-ray-tomography rendering of samples containing 0 wt% superplasticizer (W/O) and 3 wt% urea (U), 3 wt% polycarboxylate-based admixture (C), and 3 wt% naphthalene-based admixture (N) after 0 and 4 freeze-thaw cycles.

without any admixture (W/O). This is expected to affect the mechanical performance of the materials, and might be contributing to the lower compressive strength of the U and C samples compared to the W/O sample (Fig. 8). A lower flowability or higher viscosity is expected to increase the air content of the mixtures (Valcuende et al., 2012). Accordingly, before the freeze-thaw cycles the better workability of the N sample leads to smaller (Figs. 12 and 13b) and lower amounts (Fig. 13a) of air voids compared to the C sample. When aqueous solutions of urea are heated up to 80 °C, NH_3 and H_2 gasses can be released (Jones and Rollinson, 2013). These gasses might contribute to creating more voids in the U sample compared to the other samples, as observed in Figs. 11 and 13a. Despite its poor workability, the W/O sample has a low amount of air voids before the freeze-thaw cycles compared to the other samples (Figs. 11 and 13a). This might indicate that the inclusion of superplasticizers enhances air void formation which provide durability for the sample in freezing-thawing situations (Łaźniewska-Piekarczyk, 2012). In addition, the mean diameter (Fig. 13b) and pore size distribution (Fig. 12) illustrates that larger air voids are formed before the freeze-thaw cycles for the W/O and C samples compared to the N sample. This might suggest that poorer workability of the samples causes the formation of larger air voids (Sakai et al., 2006; Valcuende et al., 2012).

After 4 freeze-thaw cycles, the total volume of air voids increases significantly for the W/O and C samples while there is little change for the U and N samples (Figs. 11 and 13a). Accordingly, the

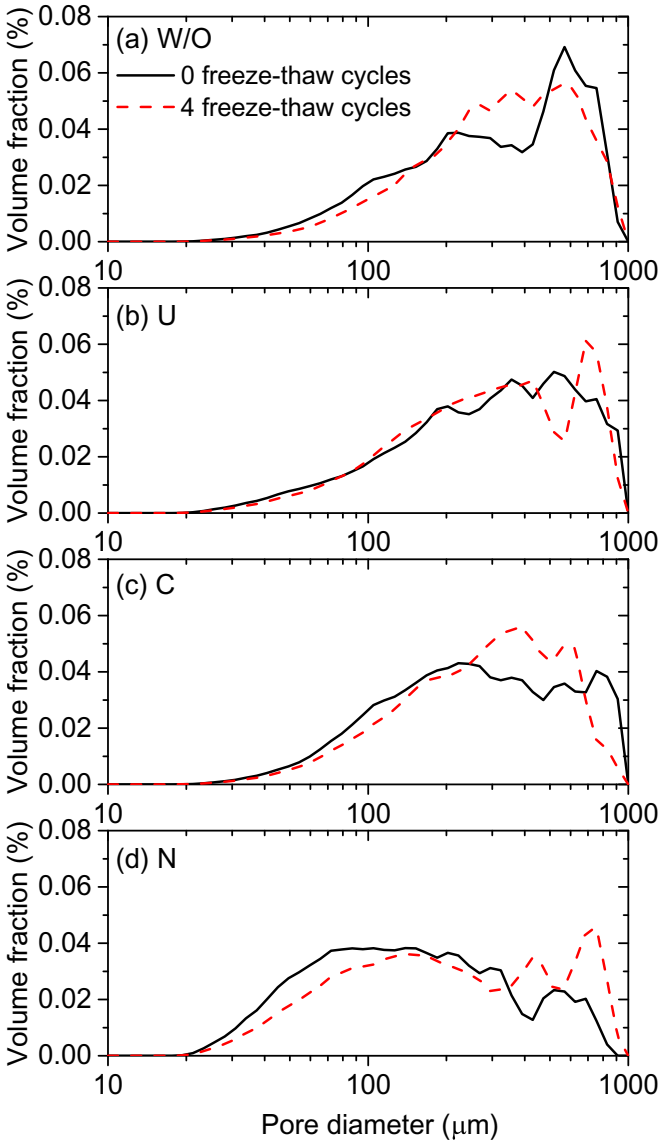

Fig. 12. Differential size distributions of air voids inside the W/O, U, C and N samples, obtained from image analyses of the X-ray-tomography images after 0 freeze-thaw cycles and 4 freeze-thaw cycles.

differences in compressive strength after the freeze-thaw process (Fig. 8) does not seem to be directly correlated with the volume of new air voids formed. This suggests that the effect of the superplasticizers on the geopolymerization reaction plays a larger role than the formation of additional air voids after the freeze-thaw cycles. As can be seen from Fig. 12, the freeze-thaw cycles seems to shift the size distributions towards larger air voids. This can both be due to an enlargement of existing voids by expansion of entrapped water, and caused by several smaller voids expanding into a common much larger void. The latter effect seems to be dominant for the N-sample, which has significantly fewer voids after the freeze-thaw cycles (Fig. 13c).

4. Conclusions

The possibility of utilizing urea (U) as a chemical admixture for lunar geopolymers was studied. The results were compared with polycarboxylate (C) and naphthalene-based (N) superplasticizers, and with a control mixture without superplasticizer (W/O). The

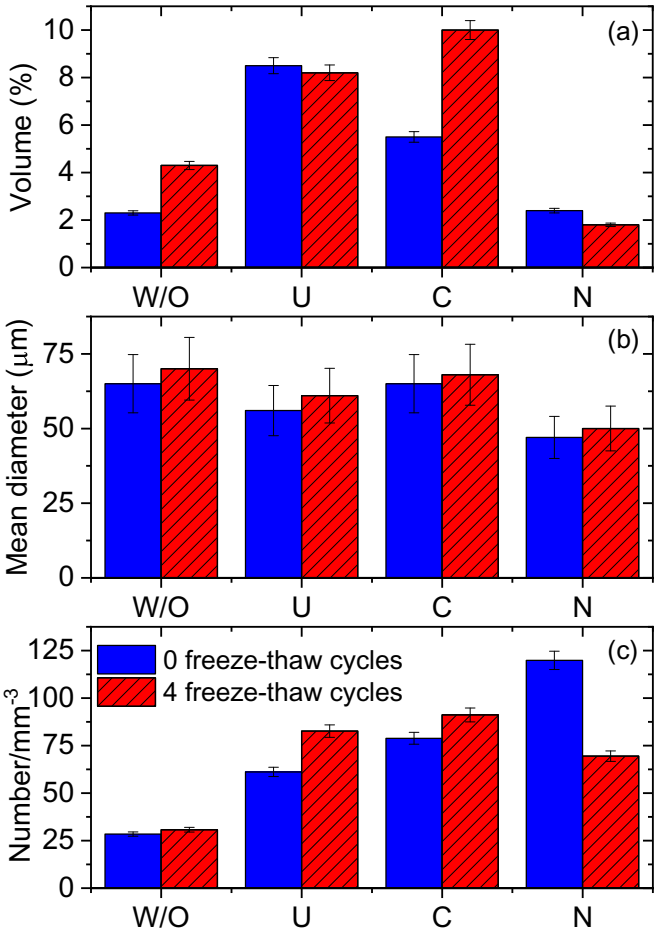

Fig. 13. (a) Volume % of air voids, (b) mean diameter of air voids, and (c) number of air voids per mm^3 for the W/O, U, C and N samples obtained from image analyses of the X-ray-tomography images after 0 freeze-thaw cycles and 4 freeze-thaw cycles.

influence of these three different powder admixtures was investigated on the physical, mechanical and microstructural properties of lunar regolith geopolymer. The following conclusions can be drawn from this work:

1. The W/O and C samples are too stiff for casting and cause the formation of fractured structures, whereas fresh U and N mixtures are castable after molding with smooth surfaces with no (U sample) or few (N sample) fractures. These U and N mixtures also retain their shape under external loads and can be pumped and built layer by layer.
2. Incorporating 3% urea postpones both initial and final setting times in comparison with mixture without any admixture. For 3D printing applications, a longer initial setting time will help maintain a continuous flow during pumping, and prevent the material from becoming too hard. For good shape retention, the fresh LG mixture should gain high early strength after extrusion to tolerate subsequent layers resting on top. In addition, urea has acceptable values of initial and final setting times.
3. The U sample exhibits a relatively high initial compressive strength (13 MPa) before freeze-thaw cycle which is more practical for 3D printing purposes than the other samples. Although, the U and N samples have the lowest compressive strength after 8 freeze-thaw cycles, they are best suited for 3D-printing.
4. FTIR show that the W/O and U samples have the highest amount of geopolymer gel formation after 0 freeze-thaw cycles, whereas

the C sample has the strongest peak after 4 freeze-thaw cycles. After 8 freeze-thaw cycles, the U sample exhibited similar intensiveness and depth of the peak as the C sample, which indicate a continuing formation of amorphous aluminosilicate gel after 8 freeze-thaw cycles.

5. 2D X-ray images show more microcracks in the U matrix after freeze-thaw cycles. This might be the cause of the lower compressive strength of the U sample. The microstructural studies also illustrate that adding superplasticizers can enhance air void formation, and thereby provide durability for the sample in freezing-thawing situations. Mean diameter and pore size distributions show that larger air voids are formed before the freeze-thaw cycles for the W/O and C samples. This can be due to the poorer workability of the samples causing the formation of larger air voids.
6. Overall urea exhibits promising properties as a superplasticizer for 3D-printing of lunar geopolymers.

Further studies are needed in order to assess how these lunar regolith geopolymers will behave under the severe lunar conditions, with a vacuum that can cause the volatile components to evaporate, and large temperature fluctuations which might cause crack formation. The ability of the geopolymers formed under these conditions to withstand meteorite bombardment, and to shield against high radiation levels should also be evaluated. In addition, 3D-printing the lunar regolith geopolymers under lunar conditions is expected to be much more challenging than it would be under normal atmospheric conditions. Additional work regarding these aspects are currently in progress.

Acknowledgement

This work is the result of an Ariadna study, a joint collaborative research project between the Faculty of Engineering at Østfold University College and the Advanced Concepts Team (ACT) of the European Space Agency (ESA). We would like to thank Rino Nilsen, Rudi Yi Xu and Andreas Erichsen for their assistance. The authors acknowledge Fundación Séneca Agencia de Ciencia y Tecnología de la Región de Murcia "Ayuda a las Unidades y Grupos de Excelencia Científica de la Región de Murcia (Programa Séneca 2014)" (Grant # 19877/GERM/14), for financial support.

References

Abdullah, M.M.A.B., Hussin, K., Bnhussain, M., Ismail, K.N., Yahya, Z., Abdul Razak, R., 2012. Fly ash-based geopolymer lightweight concrete using foaming agent. Int. J. Mol. Sci. 13 (6), 7186–7198.
Aliabdo, A.A., Abd Elmoaty, A.E.M., Salem, H.A., 2016. Effect of water addition, plasticizer and alkaline solution constitution on fly ash based geopolymer concrete performance. Constr. Build. Mater. 121, 694–703.
Allahverdi, A., Pilehvar, S., Mahinroosta, M., 2016. Influence of curing conditions on the mechanical and physical properties of chemically-activated phosphorous slag cement. Powder Technol. 288, 132–139.
Ana, M., Fernandez-Jimenez, A.P., Cecilio, L.-H., 2006. Engineering properties of alkali-activated fly ash concrete. ACI Mater. J. 103 (2), 106–112.
Bakharev, T., 2005a. Durability of geopolymer materials in sodium and magnesium sulfate solutions. Cement Concr. Res. 35 (6), 1233–1246.
Bakharev, T., 2005b. Resistance of geopolymer materials to acid attack. Cement Concr. Res. 35 (4), 658–670.
Benvenuti, S., Ceccanti, F., De Kestelier, X., 2013. Living on the moon: topological optimization of a 3D-printed lunar shelter. Nexus Netw. J. 15 (2), 285–302.
Buchner, C., Pawelke, R.H., Schlauf, T., Reissner, A., Makaya, A., 2018. A new planetary structure fabrication process using phosphoric acid. Acta Astronaut. 143, 272–284.
Buswell, R.A., de Silva, W.L., Jones, S., Dirrenberger, J., 2018. 3D printing using concrete extrusion: a roadmap for research. Cement Concr. Res. 112, 37–49.
Ceccanti, F., Dini, E., De Kestelier, X., Colla, V., Pambaguian, L., 2010. In: 3D Printing Technology for a Moon Outpost Exploiting Lunar Soil, 61st International Astronautical Congress, pp. 1–9. Prague, CZ, IAC-10-D3.
Cesaretti, G., Dini, E., De Kestelier, X., Colla, V., Pambaguian, L., 2014. Building components for an outpost on the Lunar soil by means of a novel 3D printing technology. Acta Astronaut. 93, 430–450.
Cheng, T.W., Chiu, J.P., 2003. Fire-resistant geopolymer produced by granulated blast furnace slag. Miner. Eng. 16 (3), 205–210.
Chua, K.M., Johnson, S.W., 1998. Martian and lunar cold region soil mechanics considerations. J. Aerosp. Eng. 11 (4), 138–147.
Colwell, J., Batiste, S., Horányi, M., Robertson, S., Sture, S., 2007. Lunar surface: dust dynamics and regolith mechanics. Rev. Geophys. 45 (2).
Feldkamp, L., Davis, L., Kress, J., 1984. Practical cone-beam algorithm. JOSA A 1 (6), 612–619.
Fu, Y., Cai, L., Yonggen, W., 2011. Freeze–thaw cycle test and damage mechanics models of alkali-activated slag concrete. Constr. Build. Mater. 25 (7), 3144–3148.
Happel, J.A., 1993. Indigenous materials for lunar construction. Appl. Mech. Rev. 46 (6), 313–325.
Hardjito, D., Cheak, C.C., Ing, C.H.L., 2008. Strength and setting times of low calcium fly ash-based geopolymer mortar. Mod. Appl. Sci. 2 (4), p3.
Hauri, E.H., Saal, A.E., Rutherford, M.J., Van Orman, J.A., 2015. Water in the Moon's interior: truth and consequences. Earth Planet. Sci. Lett. 409, 252–264.
Jang, J., Lee, N., Lee, H., 2014. Fresh and hardened properties of alkali-activated fly ash/slag pastes with superplasticizers. Constr. Build. Mater. 50, 169–176.
Jones, J.M., Rollinson, A.N., 2013. Thermogravimetric evolved gas analysis of urea and urea solutions with nickel alumina catalyst. Thermochim. Acta 565, 39–45.
Kong, D.L.Y., Sanjayan, J.G., 2010. Effect of elevated temperatures on geopolymer paste, mortar and concrete. Cement Concr. Res. 40 (2), 334–339.
Kosmatka, S.H., Kerkhoff, B., Panarese, W.C., MacLeod, N.F., McGrath, R.J., 2002. Design and Control of Concrete Mixtures, Seventh Canadian Edition. Cement Association of Canada, p. 151.
Le, T.T., Austin, S.A., Lim, S., Buswell, R.A., Gibb, A.G., Thorpe, T., 2012. Mix design and fresh properties for high-performance printing concrete. Mater. Struct. 45 (8), 1221–1232.
Leach, N., 2014. 3D printing in space. Architect. Des 84 (6), 108–113.
Li, Z., Ding, Z., Zhang, Y., 2004. Development of sustainable cementitious materials. In: Proceedings of International Workshop on Sustainable Development and Concrete Technology, pp. 55–76. Beijing, China.
Matta, M., Smith, S., Baumgardner, J., Wilson, J., Martinis, C., Mendillo, M., 2009. The sodium tail of the Moon. Icarus 204 (2), 409–417.
McKay, D.S., Heiken, G., Basu, A., Blanford, G., Simon, S., Reedy, R., French, B.M., Papike, J., 1991. The Lunar Regolith, Lunar Sourcebook. Camebridge University Press, Houston, Texas.
Montes, C., Broussard, K., Gongre, M., Simicevic, N., Mejia, J., Tham, J., Allouche, E., Davis, G., 2015. Evaluation of lunar regolith geopolymer binder as a radioactive shielding material for space exploration applications. Adv. Space Res. 56 (6), 1212–1221.
Ngo, T.D., Kashani, A., Imbalzano, G., Nguyen, K.T., Hui, D., 2018. Additive manufacturing (3D printing): a review of materials, methods, applications and challenges. Compos. B Eng. 143, 172–196.
Panda, B., Tan, M.J., 2018. Experimental study on mix proportion and fresh properties of fly ash based geopolymer for 3D concrete printing. Ceram. Int. 44 (9), 10258–10265.
Putnam, D.F., 1971. Composition and Concentrative Properties of Human Urine. NASA Contracror Report. NASA CR-1802.
Qiu, Y., Park, K., 2001. Environment-sensitive hydrogels for drug delivery. Adv. Drug Deliv. Rev. 53 (3), 321–339.
Rees, C.A., Provis, J.L., Lukey, G.C., Van Deventer, J.S., 2007a. In situ ATR-FTIR study of the early stages of fly ash geopolymer gel formation. Langmuir 23 (17), 9076–9082.
Rees, C.A., Provis, J.L., Lukey, G.C., van Deventer, J.S.J., 2007b. Attenuated total reflectance Fourier transform infrared analysis of fly ash geopolymer gel aging. Langmuir 23 (15), 8170–8179.
Ryu, G.S., Lee, Y.B., Koh, K.T., Chung, Y.S., 2013. The mechanical properties of fly ash-based geopolymer concrete with alkaline activators. Constr. Build. Mater. 47, 409–418.
Sakai, E., Kasuga, T., Sugiyama, T., Asaga, K., Daimon, M., 2006. Influence of superplasticizers on the hydration of cement and the pore structure of hardened cement. Cement Concr. Res. 36 (11), 2049–2053.
Schneider, C.A., Rasband, W.S., Eliceiri, K.W., 2012. NIH Image to ImageJ: 25 years of image analysis. Nat. Methods 9 (7), 671–675.
Sun, P., Wu, H.-C., 2013. Chemical and freeze–thaw resistance of fly ash-based inorganic mortars. Fuel 111, 740–745.
Usha, R., Ramasami, T., 2002. Effect of hydrogen-bond-breaking reagent (urea) on the dimensional stability of rat tail tendon (RTT) collagen fiber. J. Appl. Polym. Sci. 84 (5), 975–982.
Valcuende, M., Parra, C., Marco, E., Garrido, A., Martínez, E., Cánoves, J., 2012. Influence of limestone filler and viscosity-modifying admixture on the porous structure of self-compacting concrete. Constr. Build. Mater. 28 (1), 122–128.
Xie, J., Kayali, O., 2016. Effect of superplasticizer on workability enhancement of Class F and Class C fly ash-based geopolymers. Constr. Build. Mater. 122, 36–42.
Łaźniewska-Piekarczyk, B., 2012. The influence of selected new generation admixtures on the workability, air-voids parameters and frost-resistance of self compacting concrete. Constr. Build. Mater. 31, 310–319.